Observation of the decays $\chi_{cJ} \to \Sigma^0 \bar{p} K^+ + c.c.$ ($J = 0,1,2$)

M. Ablikim,[1] M. N. Achasov,[10,c] P. Adlarson,[67] S. Ahmed,[15] M. Albrecht,[4] R. Aliberti,[28] A. Amoroso,[66a,66c] M. R. An,[33] Q. An,[63,50] X. H. Bai,[57] Y. Bai,[49] O. Bakina,[29] R. Baldini Ferroli,[23a] I. Balossino,[24a] Y. Ban,[39,k] K. Begzsuren,[26] N. Berger,[28] M. Bertani,[23a] D. Bettoni,[24a] F. Bianchi,[66a,66c] J. Biernat,[67] J. Bloms,[60] A. Bortone,[66a,66c] I. Boyko,[29] R. A. Briere,[5] H. Cai,[68] X. Cai,[1,50] A. Calcaterra,[23a] G. F. Cao,[1,55] N. Cao,[1,55] S. A. Cetin,[54b] J. F. Chang,[1,50] W. L. Chang,[1,55] G. Chelkov,[29,b] D. Y. Chen,[6] G. Chen,[1] H. S. Chen,[1,55] M. L. Chen,[1,50] S. J. Chen,[36] X. R. Chen,[25] Y. B. Chen,[1,50] Z. J. Chen,[20,l] W. S. Cheng,[66c] G. Cibinetto,[24a] F. Cossio,[66c] X. F. Cui,[37] H. L. Dai,[1,50] X. C. Dai,[1,55] A. Dbeyssi,[15] R. E. de Boer,[4] D. Dedovich,[29] Z. Y. Deng,[1] A. Denig,[28] I. Denysenko,[29] M. Destefanis,[66a,66c] F. De Mori,[66a,66c] Y. Ding,[34] C. Dong,[37] J. Dong,[1,50] L. Y. Dong,[1,55] M. Y. Dong,[1,50,55] X. Dong,[68] S. X. Du,[71] Y. L. Fan,[68] J. Fang,[1,50] S. S. Fang,[1,55] Y. Fang,[1] R. Farinelli,[24a] L. Fava,[66b,66c] F. Feldbauer,[4] G. Felici,[23a] C. Q. Feng,[63,50] M. Fritsch,[4] C. D. Fu,[1] Y. Fu,[1] Y. Gao,[63,50] Y. Gao,[64] Y. Gao,[39,k] Y. G. Gao,[6] I. Garzia,[24a,24b] P. T. Ge,[68] C. Geng,[51] E. M. Gersabeck,[58] A. Gilman,[59] K. Goetzen,[11] L. Gong,[34] W. X. Gong,[1,50] W. Gradl,[28] M. Greco,[66a,66c] L. M. Gu,[36] M. H. Gu,[1,50] S. Gu,[2] Y. T. Gu,[13] C. Y. Guan,[1,55] A. Q. Guo,[22] L. B. Guo,[35] R. P. Guo,[41] Y. P. Guo,[9,h] A. Guskov,[29] T. T. Han,[42] W. Y. Han,[33] X. Q. Hao,[16] F. A. Harris,[56] K. L. He,[1,55] F. H. Heinsius,[4] C. H. Heinz,[28] T. Held,[4] Y. K. Heng,[1,50,55] C. Herold,[52] M. Himmelreich,[11,f] T. Holtmann,[4] Y. R. Hou,[55] Z. L. Hou,[1] H. M. Hu,[1,55] J. F. Hu,[48,m] T. Hu,[1,50,55] Y. Hu,[1] G. S. Huang,[63,50] L. Q. Huang,[64] X. T. Huang,[42] Y. P. Huang,[1] Z. Huang,[39,k] N. Huesken,[60] T. Hussain,[65] W. Ikegami Andersson,[67] W. Imoehl,[22] M. Irshad,[63,50] S. Jaeger,[4] S. Janchiv,[26,j] Q. Ji,[1] Q. P. Ji,[16] X. B. Ji,[1,55] X. L. Ji,[1,50] H. B. Jiang,[42] X. S. Jiang,[1,50,55] X. Y. Jiang,[37] J. B. Jiao,[42] Z. Jiao,[18] S. Jin,[36] Y. Jin,[57] T. Johansson,[67] N. Kalantar-Nayestanaki,[31] X. S. Kang,[34] R. Kappert,[31] M. Kavatsyuk,[31] B. C. Ke,[44,1] I. K. Keshk,[4] A. Khoukaz,[60] P. Kiese,[28] R. Kiuchi,[1] R. Kliemt,[11] L. Koch,[30] O. B. Kolcu,[54b,e] B. Kopf,[4] M. Kuemmel,[4] M. Kuessner,[4] A. Kupsc,[67] M. G. Kurth,[1,55] W. Kühn,[30] J. J. Lane,[58] J. S. Lange,[30] P. Larin,[15] A. Lavania,[21] L. Lavezzi,[66a,66c] Z. H. Lei,[63,50] H. Leithoff,[28] M. Lellmann,[28] T. Lenz,[28] C. Li,[40] C. H. Li,[33] Cheng Li,[63,50] D. M. Li,[71] F. Li,[1,50] G. Li,[1] H. Li,[44] H. Li,[63,50] H. B. Li,[1,55] H. J. Li,[9,h] J. L. Li,[42] J. Q. Li,[4] Ke Li,[1] L. K. Li,[1] Lei Li,[3] P. L. Li,[63,50] P. R. Li,[32] S. Y. Li,[53] W. D. Li,[1,55] W. G. Li,[1] X. H. Li,[63,50] X. L. Li,[42] Z. Y. Li,[51] H. Liang,[1,55] H. Liang,[63,50] Y. F. Liang,[46] Y. T. Liang,[25] L. Z. Liao,[1,55] J. Libby,[21] C. X. Lin,[51] B. J. Liu,[1] C. X. Liu,[1] D. Liu,[63,50] F. H. Liu,[45] Fang Liu,[1] Feng Liu,[6] H. B. Liu,[13] H. M. Liu,[1,55] Huanhuan Liu,[1] Huihui Liu,[17] J. B. Liu,[63,50] J. L. Liu,[64] J. Y. Liu,[1,55] K. Liu,[1] K. Y. Liu,[34] Ke Liu,[6] L. Liu,[63,50] M. H. Liu,[9,h] P. L. Liu,[1] Q. Liu,[68] Q. Liu,[55] S. B. Liu,[63,50] Shuai Liu,[47] T. Liu,[1,55] W. M. Liu,[63,50] X. Liu,[32] Y. B. Liu,[37] Z. A. Liu,[1,50,55] Z. Q. Liu,[42] X. C. Lou,[1,50,55] F. X. Lu,[16] H. J. Lu,[18] J. D. Lu,[1,55] J. G. Lu,[1,50] X. L. Lu,[1] Y. Lu,[1] Y. P. Lu,[1,50] C. L. Luo,[35] M. X. Luo,[70] P. W. Luo,[51] T. Luo,[9,h] X. L. Luo,[1,50] S. Lusso,[66c] X. R. Lyu,[55] F. C. Ma,[34] H. L. Ma,[1] L. L. Ma,[42] M. M. Ma,[1,55] Q. M. Ma,[1] R. Q. Ma,[1,55] R. T. Ma,[55] X. N. Ma,[37] X. X. Ma,[1,55] X. Y. Ma,[1,50] F. E. Maas,[15] M. Maggiora,[66a,66c] S. Maldaner,[4] S. Malde,[61] Q. A. Malik,[65] A. Mangoni,[23b] Y. J. Mao,[39,k] Z. P. Mao,[1] S. Marcello,[66a,66c] Z. X. Meng,[57] J. G. Messchendorp,[31] G. Mezzadri,[24a] T. J. Min,[36] R. E. Mitchell,[22] X. H. Mo,[1,50,55] Y. J. Mo,[6] N. Yu. Muchnoi,[10,c] H. Muramatsu,[59] S. Nakhoul,[11,f] Y. Nefedov,[29] F. Nerling,[11,f] I. B. Nikolaev,[10,c] Z. Ning,[1,50] S. Nisar,[8,i] S. L. Olsen,[55] Q. Ouyang,[1,50,55] S. Pacetti,[23b,23c] X. Pan,[9,h] Y. Pan,[58] A. Pathak,[1] P. Patteri,[23a] M. Pelizaeus,[4] H. P. Peng,[63,50] K. Peters,[11,f] J. Pettersson,[67] J. L. Ping,[35] R. G. Ping,[1,55] R. Poling,[59] V. Prasad,[63,50] H. Qi,[63,50] H. R. Qi,[53] K. H. Qi,[25] M. Qi,[36] T. Y. Qi,[2] T. Y. Qi,[9] S. Qian,[1,50] W.-B. Qian,[55] Z. Qian,[51] C. F. Qiao,[55] L. Q. Qin,[12] X. S. Qin,[4] Z. H. Qin,[1,50] J. F. Qiu,[1] S. Q. Qu,[37] K. H. Rashid,[65] K. Ravindran,[21] C. F. Redmer,[28] A. Rivetti,[66c] V. Rodin,[31] M. Rolo,[66c] G. Rong,[1,55] Ch. Rosner,[15] M. Rump,[60] H. S. Sang,[63] A. Sarantsev,[29,d] Y. Schelhaas,[28] C. Schnier,[4] K. Schoenning,[67] M. Scodeggio,[24a] D. C. Shan,[47] W. Shan,[19] X. Y. Shan,[63,50] J. F. Shangguan,[47] M. Shao,[63,50] C. P. Shen,[9] P. X. Shen,[37] X. Y. Shen,[1,55] H. C. Shi,[63,50] R. S. Shi,[1,55] X. Shi,[1,50] X. D. Shi,[63,50] W. M. Song,[27,1] Y. X. Song,[39,k] S. Sosio,[66a,66c] S. Spataro,[66a,66c] K. X. Su,[68] P. P. Su,[47] F. F. Sui,[42] G. X. Sun,[1] H. K. Sun,[1] J. F. Sun,[16] L. Sun,[68] S. S. Sun,[1,55] T. Sun,[1,55] W. Y. Sun,[35] X. Sun,[20,l] Y. J. Sun,[63,50] Y. K. Sun,[63,50] Y. Z. Sun,[1] Z. T. Sun,[1] Y. H. Tan,[68] Y. X. Tan,[63,50] C. J. Tang,[46] G. Y. Tang,[1] J. Tang,[51] J. X. Teng,[63,50] V. Thoren,[67] I. Uman,[54a] C. W. Wang,[36] D. Y. Wang,[39,k] H. P. Wang,[1,55] K. Wang,[1,50] L. L. Wang,[1] M. Wang,[42] M. Z. Wang,[39,k] Meng Wang,[1,55] W. H. Wang,[68] W. P. Wang,[63,50] X. Wang,[39,k] X. F. Wang,[32] X. L. Wang,[9,h] Y. Wang,[51] Y. Wang,[63,50] Y. D. Wang,[38] Y. F. Wang,[1,50,55] Y. Q. Wang,[1] Z. Wang,[1,50] Z. Y. Wang,[1] Ziyi Wang,[55] Zongyuan Wang,[1,55] D. H. Wei,[12] P. Weidenkaff,[28] F. Weidner,[60] S. P. Wen,[1] D. J. White,[58] U. Wiedner,[4] G. Wilkinson,[61] M. Wolke,[67] L. Wollenberg,[4] J. F. Wu,[1,55] L. H. Wu,[1] L. J. Wu,[1,55] X. Wu,[9,h] Z. Wu,[1,50] L. Xia,[63,50] H. Xiao,[9,h] S. Y. Xiao,[1] Y. J. Xiao,[1,55] Z. J. Xiao,[35] X. H. Xie,[39,k] Y. G. Xie,[1,50] Y. H. Xie,[6] T. Y. Xing,[1,55] G. F. Xu,[1] Q. J. Xu,[14] W. Xu,[1,55] X. P. Xu,[47] F. Yan,[9,h] L. Yan,[66a,66c] L. Yan,[9,h] W. B. Yan,[63,50] W. C. Yan,[71] Xu Yan,[47] H. J. Yang,[43,g] H. X. Yang,[1] L. Yang,[44] R. X. Yang,[63,50] S. L. Yang,[55] S. L. Yang,[1,55] Y. X. Yang,[12] Yifan Yang,[1,55] Zhi Yang,[25] M. Ye,[1,50] M. H. Ye,[7] J. H. Yin,[1] Z. Y. You,[51] B. X. Yu,[1,50,55] C. X. Yu,[37] G. Yu,[1,55] J. S. Yu,[20,l] T. Yu,[64] C. Z. Yuan,[1,55] L. Yuan,[2] X. Q. Yuan,[39,k] Y. Yuan,[1] Z. Y. Yuan,[51] C. X. Yue,[33] A. Yuncu,[54b,a] A. A. Zafar,[65] Y. Zeng,[20,l] B. X. Zhang,[1] Guangyi Zhang,[16] H. Zhang,[63] H. H. Zhang,[51] H. Y. Zhang,[1,50] J. J. Zhang,[44] J. L. Zhang,[69] J. Q. Zhang,[35] J. W. Zhang,[1,50,55] J. Y. Zhang,[1] J. Z. Zhang,[1,55] Jianyu Zhang,[1,55]

Jiawei Zhang,[1,55] Lei Zhang,[36] S. Zhang,[51] S. F. Zhang,[36] Shulei Zhang,[20,l] X. D. Zhang,[38] X. Y. Zhang,[42] Y. Zhang,[61] Y. H. Zhang,[1,50] Y. T. Zhang,[63,50] Yan Zhang,[63,50] Yao Zhang,[1] Yi Zhang,[9,h] Z. H. Zhang,[6] Z. Y. Zhang,[68] G. Zhao,[1] J. Zhao,[33] J. Y. Zhao,[1,55] J. Z. Zhao,[1,50] Lei Zhao,[63,50] Ling Zhao,[1] M. G. Zhao,[37] Q. Zhao,[1] S. J. Zhao,[71] Y. B. Zhao,[1,50] Y. X. Zhao,[25] Z. G. Zhao,[63,50] A. Zhemchugov,[29,b] B. Zheng,[64] J. P. Zheng,[1,50] Y. Zheng,[39,k] Y. H. Zheng,[55] B. Zhong,[35] C. Zhong,[64] L. P. Zhou,[1,55] Q. Zhou,[1,55] X. Zhou,[68] X. K. Zhou,[55] X. R. Zhou,[63,50] A. N. Zhu,[1,55] J. Zhu,[37] K. Zhu,[1] K. J. Zhu,[1,50,55] S. H. Zhu,[62] T. J. Zhu,[69] W. J. Zhu,[9,h] W. J. Zhu,[37] X. L. Zhu,[53] Y. C. Zhu,[63,50] Z. A. Zhu,[1,55] B. S. Zou,[1] and J. H. Zou[1]

(BESIII Collaboration)

[1]*Institute of High Energy Physics, Beijing 100049, People's Republic of China*
[2]*Beihang University, Beijing 100191, People's Republic of China*
[3]*Beijing Institute of Petrochemical Technology, Beijing 102617, People's Republic of China*
[4]*Bochum Ruhr-University, D-44780 Bochum, Germany*
[5]*Carnegie Mellon University, Pittsburgh, Pennsylvania 15213, USA*
[6]*Central China Normal University, Wuhan 430079, People's Republic of China*
[7]*China Center of Advanced Science and Technology, Beijing 100190, People's Republic of China*
[8]*COMSATS University Islamabad, Lahore Campus, Defence Road,
Off Raiwind Road, 54000 Lahore, Pakistan*
[9]*Fudan University, Shanghai 200443, People's Republic of China*
[10]*G.I. Budker Institute of Nuclear Physics SB RAS (BINP), Novosibirsk 630090, Russia*
[11]*GSI Helmholtzcentre for Heavy Ion Research GmbH, D-64291 Darmstadt, Germany*
[12]*Guangxi Normal University, Guilin 541004, People's Republic of China*
[13]*Guangxi University, Nanning 530004, People's Republic of China*
[14]*Hangzhou Normal University, Hangzhou 310036, People's Republic of China*
[15]*Helmholtz Institute Mainz, Johann-Joachim-Becher-Weg 45, D-55099 Mainz, Germany*
[16]*Henan Normal University, Xinxiang 453007, People's Republic of China*
[17]*Henan University of Science and Technology, Luoyang 471003, People's Republic of China*
[18]*Huangshan College, Huangshan 245000, People's Republic of China*
[19]*Hunan Normal University, Changsha 410081, People's Republic of China*
[20]*Hunan University, Changsha 410082, People's Republic of China*
[21]*Indian Institute of Technology Madras, Chennai 600036, India*
[22]*Indiana University, Bloomington, Indiana 47405, USA*
[23a]*INFN Laboratori Nazionali di Frascati, INFN Laboratori Nazionali di Frascati, I-00044 Frascati, Italy*
[23b]*INFN Laboratori Nazionali di Frascati, INFN Sezione di Perugia, I-06100, Perugia, Italy*
[23c]*INFN Laboratori Nazionali di Frascati, University of Perugia, I-06100, Perugia, Italy*
[24a]*INFN Sezione di Ferrara, INFN Sezione di Ferrara, I-44122, Ferrara, Italy*
[24b]*INFN Sezione di Ferrara, University of Ferrara, I-44122, Ferrara, Italy*
[25]*Institute of Modern Physics, Lanzhou 730000, People's Republic of China*
[26]*Institute of Physics and Technology, Peace Ave. 54B, Ulaanbaatar 13330, Mongolia*
[27]*Jilin University, Changchun 130012, People's Republic of China*
[28]*Johannes Gutenberg University of Mainz, Johann-Joachim-Becher-Weg 45, D-55099 Mainz, Germany*
[29]*Joint Institute for Nuclear Research, 141980 Dubna, Moscow region, Russia*
[30]*Justus-Liebig-Universitaet Giessen, II. Physikalisches Institut, Heinrich-Buff-Ring 16,
D-35392 Giessen, Germany*
[31]*KVI-CART, University of Groningen, NL-9747 AA Groningen, Netherlands*
[32]*Lanzhou University, Lanzhou 730000, People's Republic of China*
[33]*Liaoning Normal University, Dalian 116029, People's Republic of China*
[34]*Liaoning University, Shenyang 110036, People's Republic of China*
[35]*Nanjing Normal University, Nanjing 210023, People's Republic of China*
[36]*Nanjing University, Nanjing 210093, People's Republic of China*
[37]*Nankai University, Tianjin 300071, People's Republic of China*
[38]*North China Electric Power University, Beijing 102206, People's Republic of China*
[39]*Peking University, Beijing 100871, People's Republic of China*
[40]*Qufu Normal University, Qufu 273165, People's Republic of China*
[41]*Shandong Normal University, Jinan 250014, People's Republic of China*
[42]*Shandong University, Jinan 250100, People's Republic of China*
[43]*Shanghai Jiao Tong University, Shanghai 200240, People's Republic of China*
[44]*Shanxi Normal University, Linfen 041004, People's Republic of China*

[45]*Shanxi University, Taiyuan 030006, People's Republic of China*

[46]*Sichuan University, Chengdu 610064, People's Republic of China*

[47]*Soochow University, Suzhou 215006, People's Republic of China*

[48]*South China Normal University, Guangzhou 510006, People's Republic of China*

[49]*Southeast University, Nanjing 211100, People's Republic of China*

[50]*State Key Laboratory of Particle Detection and Electronics, Beijing 100049,*
Hefei 230026, People's Republic of China

[51]*Sun Yat-Sen University, Guangzhou 510275, People's Republic of China*

[52]*Suranaree University of Technology, University Avenue 111,*
Nakhon Ratchasima 30000, Thailand

[53]*Tsinghua University, Beijing 100084, People's Republic of China*

[54a]*Turkish Accelerator Center Particle Factory Group, Istanbul Bilgi University,*
34060 Eyup, Istanbul, Turkey

[54b]*Turkish Accelerator Center Particle Factory Group, Near East University, Nicosia, North Cyprus,*
Mersin 10, Turkey

[55]*University of Chinese Academy of Sciences, Beijing 100049, People's Republic of China*

[56]*University of Hawaii, Honolulu, Hawaii 96822, USA*

[57]*University of Jinan, Jinan 250022, People's Republic of China*

[58]*University of Manchester, Oxford Road, Manchester M13 9PL, United Kingdom*

[59]*University of Minnesota, Minneapolis, Minnesota 55455, USA*

[60]*University of Muenster, Wilhelm-Klemm-Str. 9, 48149 Muenster, Germany*

[61]*University of Oxford, Keble Rd, Oxford OX13RH, United Kingdom*

[62]*University of Science and Technology Liaoning, Anshan 114051, People's Republic of China*

[63]*University of Science and Technology of China, Hefei 230026, People's Republic of China*

[64]*University of South China, Hengyang 421001, People's Republic of China*

[65]*University of the Punjab, Lahore-54590, Pakistan*

[66a]*University of Turin and INFN, University of Turin, I-10125, Turin, Italy*

[66b]*University of Turin and INFN, University of Eastern Piedmont, I-15121, Alessandria, Italy*

[66c]*University of Turin and INFN, INFN, I-10125, Turin, Italy*

[67]*Uppsala University, Box 516, SE-75120 Uppsala, Sweden*

[68]*Wuhan University, Wuhan 430072, People's Republic of China*

[69]*Xinyang Normal University, Xinyang 464000, People's Republic of China*

[70]*Zhejiang University, Hangzhou 310027, People's Republic of China*

[71]*Zhengzhou University, Zhengzhou 450001, People's Republic of China*

The decays $\chi_{cJ} \to \Sigma^0 \bar{p} K^+$ + c.c. $(J = 0, 1, 2)$ are studied via the radiative transition $\psi(3686) \to \gamma \chi_{cJ}$ based on a data sample of $(448.1 \pm 2.9) \times 10^6$ $\psi(3686)$ events collected with the BESIII detector. The branching fractions of $\chi_{cJ} \to \Sigma^0 \bar{p} K^+$ + c.c. $(J = 0, 1, 2)$ are measured to be $(3.03 \pm 0.12 \pm 0.15) \times 10^{-4}$,

[a]Also at Bogazici University, 34342 Istanbul, Turkey.

[b]Also at the Moscow Institute of Physics and Technology, Moscow 141700, Russia.

[c]Also at the Novosibirsk State University, Novosibirsk, 630090, Russia.

[d]Also at the NRC "Kurchatov Institute", PNPI, 188300, Gatchina, Russia.

[e]Also at Istanbul Arel University, 34295 Istanbul, Turkey.

[f]Also at Goethe University Frankfurt, 60323 Frankfurt am Main, Germany.

[g]Also at Key Laboratory for Particle Physics, Astrophysics and Cosmology, Ministry of Education; Shanghai Key Laboratory for Particle Physics and Cosmology; Institute of Nuclear and Particle Physics, Shanghai 200240, People's Republic of China.

[h]Also at Key Laboratory of Nuclear Physics and Ion-beam Application (MOE) and Institute of Modern Physics, Fudan University, Shanghai 200443, People's Republic of China.

[i]Also at Harvard University, Department of Physics, Cambridge, MA, 02138, USA.

[j]Currently at: Institute of Physics and Technology, Peace Ave.54B, Ulaanbaatar 13330, Mongolia.

[k]Also at State Key Laboratory of Nuclear Physics and Technology, Peking University, Beijing 100871, People's Republic of China.

[l]School of Physics and Electronics, Hunan University, Changsha 410082, China.

[m]Also at Guangdong Provincial Key Laboratory of Nuclear Science, Institute of Quantum Matter, South China Normal University, Guangzhou 510006, China.

$(1.46 \pm 0.07 \pm 0.07) \times 10^{-4}$, and $(0.91 \pm 0.06 \pm 0.05) \times 10^{-4}$, respectively, where the first uncertainties are statistical and the second are systematic. In addition, no evident structure is found for excited baryon resonances on the two-body subsystems with the limited statistics.

I. INTRODUCTION

The P-wave charmonia χ_{cJ} $(J = 0, 1, 2)$ have been observed experimentally for a long time, however, most decay modes of them are still unknown. Though χ_{cJ} cannot be directly produced via electron-positron annihilation into a virtual photon, radiative decays of the $\psi(3686)$ into χ_{cJ} states make up about 10% of the total decay width of the $\psi(3686)$ for each χ_{cJ} [1]. Thus, the large $\psi(3686)$ data sample containing $(448.1 \pm 2.9) \times 10^6$ events at BESIII can ideally be used to investigate χ_{cJ} decays [2,3].

Many two-body decays of $\chi_{cJ} \rightarrow B\bar{B}$ have been observed in experiments, but three-body decays of $\chi_{cJ} \rightarrow B\bar{B}M$ are much less measured (B stands for a baryon, M stands for a meson), while the latter have advantages to search for and study excited baryons due to larger freedom of quantum numbers. For example, some experiments reported two excited Σ resonances around 1670 MeV/c^2, which have the same mass and J^{PC} quantum numbers but very different decay products and angular distributions [4–7]. Further experimental information will shed light on the understanding of these states.

The decays of $\chi_{cJ} \rightarrow \Sigma^+ \bar{p} K_S^0$ $(J = 0, 1, 2)^1$ have been measured at BESIII [8], which implies the existence of isospin conjugate channels $\chi_{cJ} \rightarrow \Sigma^0 \bar{p} K^+$ $(J = 0, 1, 2)$. The decays of $\chi_{cJ} \rightarrow \Sigma^0 \bar{p} K^+$ $(J = 0, 1, 2)$ can be used to search for the excited Σ resonances and understand their properties.

In this analysis, we present a study of $\psi(3686) \rightarrow \gamma\chi_{cJ}$, $\chi_{cJ} \rightarrow \Sigma^0 \bar{p} K^+$ $(J = 0, 1, 2)$, where Σ^0 is reconstructed in its dominant decay mode $\Sigma^0 \rightarrow \gamma\Lambda$ with $\Lambda \rightarrow p\pi^-$.

II. BESIII DETECTOR

The BESIII detector [9] records symmetric e^+e^- collisions provided by the BEPCII storage ring [10], which operates with a peak luminosity of 1×10^{33} cm^{-2} s^{-1} in the center-of-mass energy range from 2.0 to 4.7 GeV. The cylindrical core of the BESIII detector consists of a helium-based multilayer drift chamber (MDC), a plastic scintillator time-of-flight system (TOF), and a CsI (Tl) electromagnetic calorimeter (EMC), which are all enclosed in a superconducting solenoidal magnet providing a 1.0 T magnetic field. The solenoid is supported by an octagonal flux-return yoke with resistive plate counter muon identifier modules interleaved with steel. The charged-particle momentum

---

[1]Throughout this paper, charge conjugate is implied unless otherwise stated.

resolution at 1 GeV/c is 0.5%, and the dE/dx resolution is 6% for the electrons of 1 GeV/c momentum. The EMC measures photon energies with a resolution of 2.5% (5%) at 1 GeV in the barrel (end cap) region. The time resolution of the TOF barrel part is 68 ps, while that of the end cap part is 110 ps.

III. DATASET AND MONTE CARLO SIMULATION

This analysis is based on a sample of $(448.1 \pm 2.9) \times 10^6$ $\psi(3686)$ events [11] collected with the BESIII detector.

Simulated data samples produced with a GEANT4-based [12] Monte Carlo (MC) package, which includes the geometric description of the BESIII detector and the detector response, are used to determine detection efficiencies and to estimate backgrounds. The simulation models the beam energy spread and initial state radiation (ISR) in the e^+e^- annihilations with the generator KKMC [13,14]. The inclusive MC sample includes 506×10^6 $\psi(3686)$ events, the ISR production of the J/ψ, and the continuum processes incorporated in KKMC. The known decay modes are modeled with EVTGEN [15,16] using branching fractions taken from the Particle Data Group [1], and the remaining unknown charmonium decays are modeled with LUNDCHARM [17]. Final state radiation (FSR) from charged particles is incorporated using the PHOTOS package [18].

The decays of $\psi(3686) \rightarrow \gamma\chi_{cJ}(J = 0, 1, 2)$ are simulated following Ref. [19], in which the magnetic-quadrupole (M2) transition for $\psi(3686) \rightarrow \gamma\chi_{c1,2}$ and the electric-octupole (E3) transition for $\psi(3686) \rightarrow \gamma\chi_{c2}$ are considered in addition to the dominant electric-dipole (E1) transition. The three-body decays $\chi_{cJ} \rightarrow \Sigma^0 \bar{p} K^+$ are generated evenly distributed in phase-space (PHSP).

IV. EVENT SELECTION AND BACKGROUND ANALYSIS

For $\psi(3686) \rightarrow \gamma\chi_{cJ}$, $\chi_{cJ} \rightarrow \Sigma^0 \bar{p} K^+$ with $\Sigma^0 \rightarrow \gamma\Lambda$ and $\Lambda \rightarrow p\pi^-$, the final state consists of $p\bar{p}K^+\pi^-\gamma\gamma$. Charged tracks must be in the active region of the MDC, corresponding to $|\cos\theta| < 0.93$, where θ is the polar angle of the charged track with respect to the symmetry axis of the detector. For the two charged tracks from the Λ decay, the distance between their point of closest approach and the primary vertex is required to be less than 20 cm along the beam direction, and less than 10 cm in the plane perpendicular to the beam direction. For the remaining charged tracks, the same distance is required to be less than 10 cm along the beam direction and less than 1 cm in the
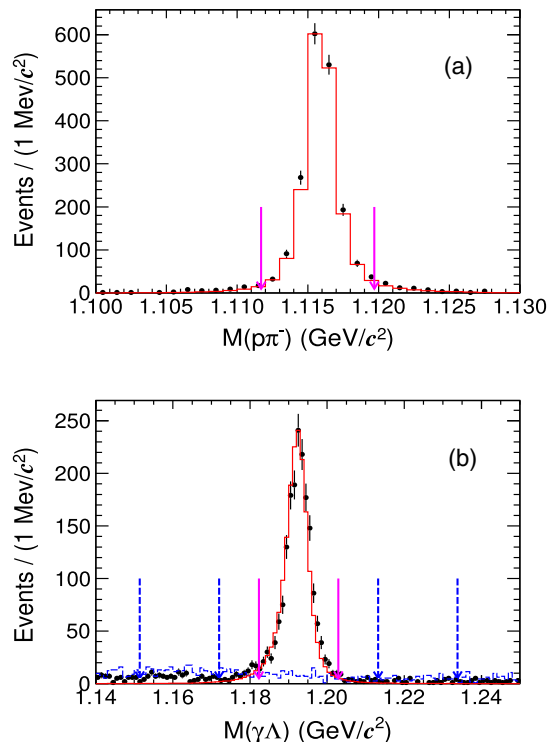
FIG. 1. (a) The distribution of the $p\pi$ invariant mass. (b) The distribution of the $\gamma\Lambda$ invariant mass. The solid arrows respectively show the Λ and Σ^0 mass windows, and the dashed arrows show the Σ^0 sideband mass regions. Dots with error bars are data, the histograms with solid lines represent signal MC simulations, and the dashed line in (b) is the background contribution from the inclusive MC sample scaled to the total number of $\psi(3686)$ events.
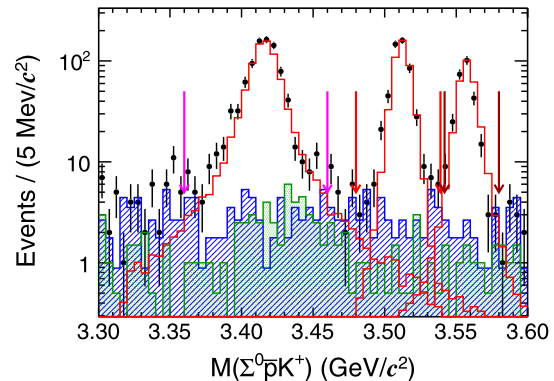
FIG. 2. The distribution of the $\Sigma^0\bar{p}K^+$ invariant mass in the region of the χ_{cJ} states. The dots with error bars are data, the solid histogram is the χ_{cJ} line shape from MC simulations, the hatched histogram is the background contribution from the inclusive MC sample, where the signal MC simulations and inclusive MC sample have been normalized to the data luminosity. The dot-shade histogram is the normalized Σ^0 sideband, and the solid arrows indicate the χ_{c0}, χ_{c1}, and χ_{c2} signal regions.

plane perpendicular to the beam direction. The total number of charged tracks needs to be equal to or greater than four.

The TOF and dE/dx information is used to calculate a particle identification (PID) likelihood (P) for the hypotheses that a track is a pion, kaon, or proton. Tracks from the primary vertex are required to be identified as either an antiproton ($P(p) > P(K)$ and $P(p) > P(\pi)$) or a kaon ($P(K) > P(p)$ and $P(K) > P(\pi)$). In case of daughter particles of a Λ candidate, the track with the larger momentum is identified as the proton, and the other is identified as the pion. For each candidate event, exactly one $\bar{p}, K^+$, and p, π^- from the Λ decay are required.

For all combinations of positively and negatively charged tracks, secondary vertex fits are performed [20], and the combination with the smallest χ_Λ^2 is retained as the Λ candidate. In addition, the ratio of the decay length (L) to its resolution (σ_L) is required to be larger than zero. The mass distribution of the reconstructed Λ candidates is shown in Fig. 1(a). A mass window of $|M_{p\pi^-} - m_\Lambda| < 0.004$ GeV/c^2 is required to select the Λ signal events, where $M_{p\pi^-}$ is the invariant mass of selected proton-pion pairs and m_Λ is the nominal mass of Λ taken from the PDG [1].

Photon candidates are reconstructed from the energy deposition in the EMC crystals produced by electromagnetic showers. The minimum energy requirement for a photon candidate is 25 MeV in the barrel region ($|\cos\theta| < 0.80$) and 50 MeV in the end cap region ($0.86 < |\cos\theta| < 0.92$). To eliminate showers originating from charged particles, a photon cluster must be separated by at least 10° from any charged tracks. The time-information of the shower is required to be within 700 ns from the reconstructed event start-time to suppress noise and energy deposits unrelated to the event. The total number of photons is required to be at least two. To reduce background events from $\pi^0 \to \gamma\gamma$, we require $|M_{\gamma\gamma} - m_{\pi^0}| > 0.015$ GeV/c^2.

A four-constraint (4C) kinematic fit imposing four-momentum conservation is performed using the $p\bar{p}K^+\pi^-\gamma\gamma$ hypothesis. If there are more than two photon candidates in one event, the combination with the smallest χ_{4C}^2 is retained, and its χ_{4C}^2 is required to be smaller than those for the alternative $p\bar{p}K^+\pi^-\gamma$ and $p\bar{p}K^+\pi^-\gamma\gamma\gamma$ hypotheses. In addition, the value of χ_{4C}^2 is required to be less than 40. For the selected signal candidates, the $\gamma\Lambda$ combination with the invariant mass closest to the nominal Σ^0 mass according to the PDG [1] is taken as the Σ^0 candidate. The distribution of the $\gamma\Lambda$ invariant mass is shown in Fig. 1(b). The Σ^0 signal region is defined as $|M_{\gamma\Lambda} - m_{\Sigma^0}| < 0.010$ GeV/c^2, while the sideband regions are defined as $[1.151, 1.172]$ GeV/c^2 and $[1.213, 1.234]$ GeV/c^2 as indicated by the dashed arrows in Fig. 1(b).

The $\Sigma^0\bar{p}K^+$ invariant mass distribution after application of all selection conditions is shown in Fig. 2, where clear χ_{c0}, χ_{c1}, and χ_{c2} signals are observed. The signal MC simulation also shown in Fig. 2 agrees with the data very well.

The $\psi(3686)$ inclusive MC sample is used to study possible peaking backgrounds. Applying the same requirements as the data, the two main remaining background
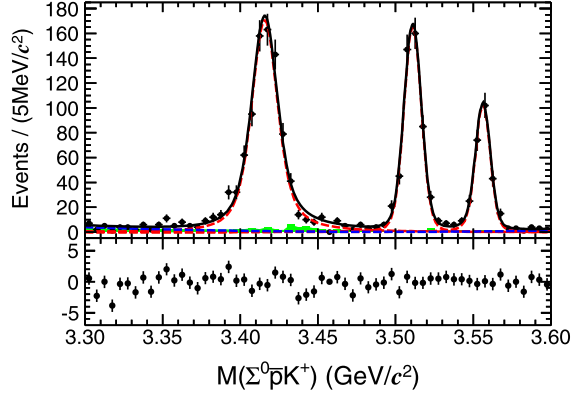
FIG. 3. Fit to the $M(\Sigma^0 \bar{p} K^+)$ spectrum. Dots with error bars correspond to the data, the black solid curve shows the fit result, the red dashed lines are the signal shapes of the χ_{cJ} states, the green shaded histogram is the normalized Σ^0 sideband contribution, and the blue dashed line is the continuum background.

channels involve either $\psi(3686) \to K^{*+} \bar{p} \Lambda$ with $K^{*+} \to K^+ \pi^0$ ($\pi^0 \to \gamma\gamma$) decays or belong to the peaking background channel $\psi(3686) \to \gamma\chi_{cJ} \to \gamma K^+ \bar{p} \Lambda$ ($\Lambda \to p\pi^-$) that is missing the intermediate Σ^0 decay. Other small backgrounds are smoothly distributed below the χ_{cJ} signal region. All the backgrounds can also be estimated by the Σ^0 sideband events normalized to the background in the Σ^0 signal region. The normalized sideband events are shown as the dot-shade histogram in Fig. 2.

V. MEASUREMENT OF $\mathcal{B}(\chi_{cJ} \to \Sigma^0 \bar{p} K^+ + \mathrm{c.c.})$

The result of an unbinned maximum likelihood fit to the $M_{\Sigma^0 \bar{p} K^+}$ distribution is shown in Fig. 3. Here, we fit $\sum_J (N_{1,J} \cdot f_{\mathrm{signal}}^J) + \sum_J (N_{2,J} \cdot f_{\mathrm{peakbkg}}^J) + N_3 \cdot f_{\mathrm{flatbkg}}$, where f_{signal}^J is the probability density function describing the χ_{cJ} resonances, f_{peakbkg}^J is the normalized shape of the Σ^0 sidebands, and f_{flatbkg} is given by a second-order polynomial. The line shape of each resonance f_{signal} is modeled with the same formula $BW(M) \cdot E_\gamma^3 \cdot D(E_\gamma)$ as in Ref. [8], where M is the $\Sigma^0 \bar{p} K^+$ invariant mass, $BW(M) = \frac{1}{(M - m_{\chi_{cJ}})^2 + (\frac{\Gamma_{\chi_{cJ}}}{2})^2}$ is the Breit-Wigner function, $\Gamma_{\chi_{cJ}}$ is the width of the corresponding χ_{cJ}, $E_\gamma = \frac{m_{\psi(3686)}^2 - M^2}{2m_{\psi(3686)}}$ is the energy of the transition photon in the rest frame of the $\psi(3686)$, and $D(E_\gamma)$ is the damping factor which suppresses the divergent tail due to the E_γ^3 dependence of f_{signal}^J. It is described by $\exp(-E_\gamma^2/8\beta^2)$, where $\beta = (65.0 \pm 2.5)$ MeV was measured by the CLEO experiment [21]. The signal shapes are convolved with Gaussian functions to account for the mass resolution.

The parameters $N_{1,J}$, N_3 and two coefficients of the polynomial are taken as the free parameters in the fit, while $N_{2,J}$ is fixed to the number of the normalized Σ^0 sideband events. In the description of f_{signal}^J, the masses and widths

TABLE I. Summary of the number of fitted signal events (N^{obs}), detection efficiency (ϵ), and branching fraction $\mathcal{B}(\chi_{cJ} \to \Sigma^0 \bar{p} K^+)$, where the first uncertainty is statistical and the second one is systematic.

Mode	N^{obs}	$\epsilon(\%)$	$\mathcal{B}(\chi_{cJ} \to \Sigma^0 \bar{p} K^+)(10^{-4})$
$\chi_{c0} \to \Sigma^0 \bar{p} K^+$	871 ± 34	10.25 ± 0.05	$3.03 \pm 0.12 \pm 0.15$
$\chi_{c1} \to \Sigma^0 \bar{p} K^+$	493 ± 24	12.12 ± 0.05	$1.46 \pm 0.07 \pm 0.07$
$\chi_{c2} \to \Sigma^0 \bar{p} K^+$	271 ± 18	10.90 ± 0.05	$0.91 \pm 0.06 \pm 0.05$

of the χ_{cJ} states are fixed to the PDG values. The Gaussian resolution parameters in the region of the three χ_{cJ} states are also free parameters, and are found to be 5.7, 5.1, and 4.1 MeV/c^2 for χ_{c0}, χ_{c1}, and χ_{c2}, respectively. The yields of signal events of all three $\chi_{cJ} \to \Sigma^0 \bar{p} K^+$ decays are listed in Table I.

Dalitz plots and the one dimensional projections of $\chi_{cJ} \to \Sigma^0 \bar{p} K^+$ events are shown in the left, middle and right columns of Fig. 4 for the χ_{c0}, χ_{c1}, and χ_{c2} signal regions, respectively, together with the distributions of MC simulated signal events based on a pure phase-space decay model.

For $\bar{p} K^+$ mass spectra of the data, it seems there are two structures around 1.7 and 2.0 GeV/c^2 for χ_{c0} decays, they are likely $\bar{\Sigma}(1750)^0$ and $\bar{\Sigma}(1940)^0$. There seems to be two structures around 1.9 GeV/c^2 for χ_{c1} decays and around 1.8 GeV/c^2 for χ_{c2} decays. For $\Sigma^0 K^+$ mass spectra, it seems there is a jump around 1.8 GeV/c^2 and a dip around 2.0 GeV/c^2 for χ_{c0} decays, the jump may be $N(1880)$ with $J^P = \frac{1}{2}^+$ or $N(1895)$ with $J^P = \frac{1}{2}^-$. There is an indication around 1.95 GeV/c^2 for χ_{c1} decays, which may be $N(1900)$ with $J^P = \frac{3}{2}^+$. There is no evident structure for χ_{c2} decays. For $\Sigma^0 \bar{p}$ mass spectra, the data are consistent with the phase-space MC shapes, there is no evident structure for χ_{c0}, χ_{c1}, and χ_{c2} decays. The mass distributions of two-body subsystems of the data are not completely consistent with the phase-space MC simulations, but it is difficult to draw any conclusions to them due to present limited statistics.

The differences between data and MC simulation indicate that these signal MC events cannot be used to calculate the selection efficiency directly. Instead, the detection efficiency is obtained by weighting the simulated Dalitz plot distribution with the distribution from data. We divide the Dalitz plots of $M_{\bar{p}K^+}^2$ versus $M_{\Sigma^0 K^+}^2$ into 12×12, 8×7, and 6×8 bins in the χ_{c0}, χ_{c1}, and χ_{c2} regions, respectively. First, we obtain the weight factor ω_i in each bin as the ratio between the Dalitz plot distribution of data and the normalized signal MC sample. In a second step, ω_i is used to correct the Dalitz distributions of both the generated and reconstructed MC simulations. Finally, we determine the corrected detection efficiency as the ratio between the sum of event weights in reconstructed and generated MC. The results are listed in Table I.
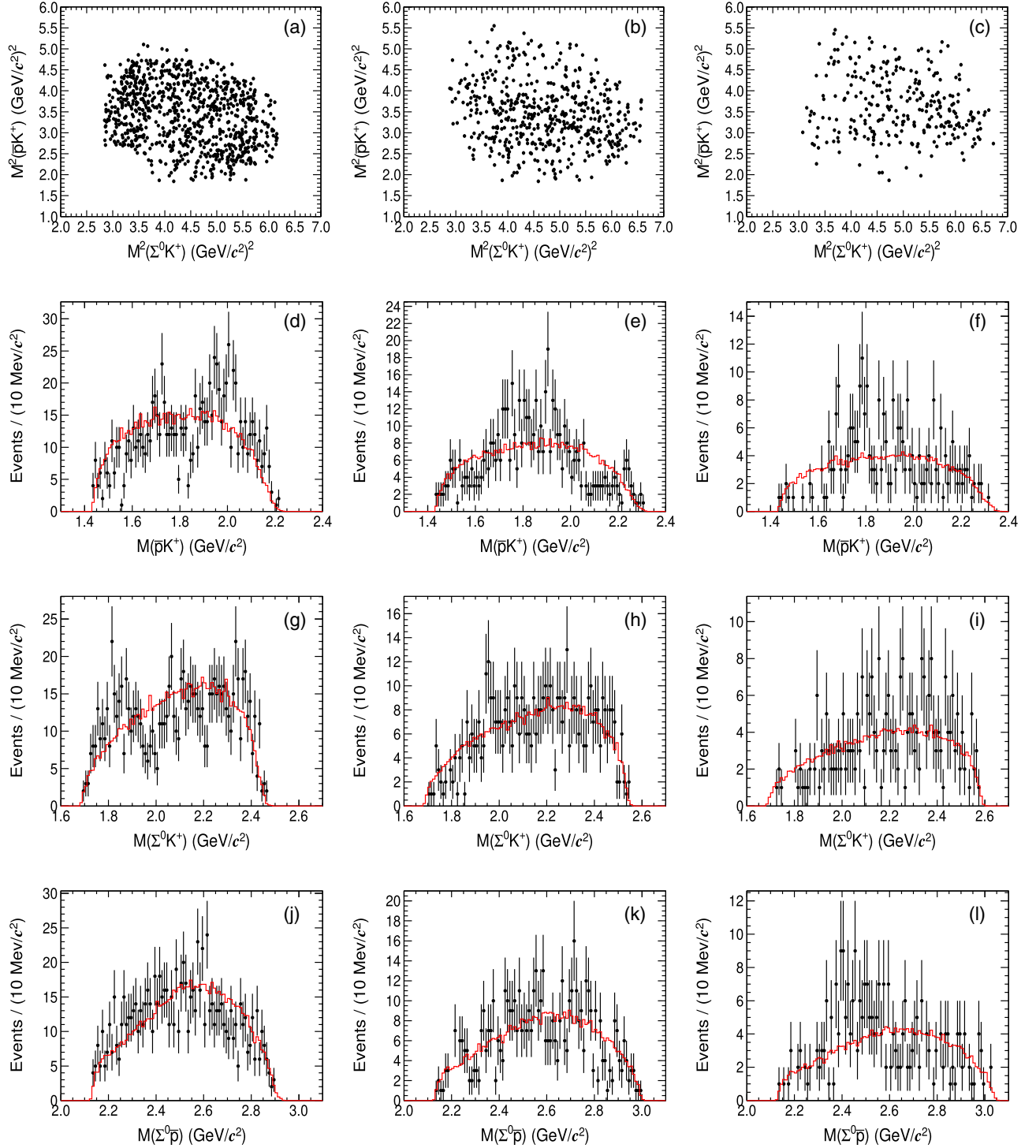
FIG. 4. Dalitz plots and one-dimensional projections of $\chi_{cJ} \to \Sigma^0 \bar{p} K^+$ ($J = 0, 1, 2$). The left column (a, d, g, j) is for χ_{c0}, the middle column (b, e, h, k) is for χ_{c1}, and the right column (c, f, i, l) is for χ_{c2}. Dots with error bars are the data, the histograms with solid lines represent phase-space MC simulations.

The branching fractions for $\chi_{cJ} \to \Sigma^0 \bar{p} K^+$ are calculated using

$$\mathcal{B}(\chi_{cJ} \to \Sigma^0 \bar{p} K^+) = \frac{N^{\text{obs}}}{N_{\psi(3686)} \cdot \epsilon \cdot \prod_j \mathcal{B}_j}, \quad (1)$$

where N^{obs} is the number of signal events obtained from the fit, $N_{\psi(3686)}$ is the total number of $\psi(3686)$ events, ϵ is the corresponding detection efficiency as listed in Table I, and $\prod_j \mathcal{B}_j = \mathcal{B}(\psi(3686) \to \gamma\chi_{cJ}) \times \mathcal{B}(\Sigma^0 \to \gamma\Lambda) \times \mathcal{B}(\Lambda \to p\pi^-)$ is the product branching

fraction with individual values taken from the PDG [1]. The results for $\chi_{cJ} \to \Sigma^0 \bar{p} K^+ (J = 0, 1, 2)$ are listed in Table I.

VI. SYSTEMATIC UNCERTAINTIES

The systematic uncertainties on the measurement of the branching fractions of $\chi_{cJ} \to \Sigma^0 \bar{p} K^+$ are discussed below.

Using the control samples of $J/\psi \to p\bar{p}\pi^+\pi^-$ and $J/\psi \to K^*\bar{K}$, the difference of tracking efficiencies between MC simulation and data is within 1% for $\bar{p}$ and K^+. Therefore, 2% is taken as the tracking systematic uncertainty.

The $\bar{p}/K^+$ PID efficiency is studied using $J/\psi \to p\bar{p}\pi^+\pi^-$ and $J/\psi \to K_S^0 K^\pm \pi^\pm$ control samples [22,23], with the result being that the PID efficiency for data agrees with that of the MC simulation within 1% per $\bar{p}/K^+$. So 2% is taken as the systematic uncertainty associated with the PID efficiency.

The photon detection efficiency is studied from a $J/\psi \to \pi^+\pi^-\pi^0$ control sample [24]. The efficiency difference between data and MC simulation is about 1% per photon, so that 2% is assigned as the systematic uncertainty from the two photons.

In order to determine the uncertainty associated with the secondary vertex fit and the decay length requirement, we determine the efficiency of these selection criteria by comparing the $\Lambda \to p\pi^-$ signal yields with and without those selections for both data and signal MC. From a fit to the $p\pi^-$ invariant mass distributions, we find a data-MC difference of 0.7% that is assigned as the systematic uncertainty. For each track stemming from $\Lambda \to p\pi^-$ decays, the systematic uncertainty from the tracking efficiency is 1.0% according to an analysis of $J/\psi \to \bar{p} K^+ \Lambda$ [25]. The total uncertainty of the Λ reconstruction is 2.1%.

The uncertainty associated with the 4C kinematic fit comes from a potential inconsistency between data and MC simulation; this difference is reduced by correcting the track helix parameters in the MC simulation, as described in detail in Ref. [26]. The difference of the efficiency with and without the helix correction is considered as the systematic uncertainty from the kinematic fit.

The uncertainty related to the Λ and Σ^0 mass windows is studied by determining the yield of Λ (Σ^0) inside the mass windows for both data and signal MC simulation. The difference between data and MC simulation is found to be negligible for Λ, and to be 0.2% for Σ^0.

In the weighting procedure, the Dalitz plots were divided into 12×12, 8×7 and 6×8 bins in order to calculate the event-weights used in the efficiency determination. We repeat this procedure with different bin configurations. The maximum difference between the nominal binning and the alternate configuration is taken as the weighting related uncertainty listed in Table II. The statistical uncertainty of the efficiency is determined

TABLE II. Summary of systematic uncertainty sources and their contributions (in %).

Source	$\mathcal{B}(\chi_{c0})$	$\mathcal{B}(\chi_{c1})$	$\mathcal{B}(\chi_{c2})$
Tracking	2.0	2.0	2.0
PID	2.0	2.0	2.0
Photon detection	2.0	2.0	2.0
Λ reconstruction	2.1	2.1	2.1
4C kinematic fit	0.7	0.1	1.0
Λ mass window	⋯	⋯	⋯
Σ^0 mass window	0.2	0.2	0.2
Weighting procedure	1.2	0.3	1.0
MC statistics	0.5	0.5	0.5
Fitting procedure	1.4	1.1	1.0
Secondary branching fractions	2.2	2.6	2.2
Number of $\psi(3686)$	0.6	0.6	0.6
Total	5.1	5.0	5.0

directly from MC simulations and amounts to less than 0.5%.

The systematic uncertainty related to the fitting procedure includes multiple sources. Concerning the signal line shape, the damping factor is changed from $\exp(-E_\gamma^2/8\beta^2)$ as used by CLEO to $\frac{E_0^2}{E_0 E_\gamma + (E_0 - E_\gamma)^2}$ as used by KEDR [27]. The resulting differences in the fit are assigned as the systematic uncertainties. In addition, the fit range is varied from $[3.30, 3.60]$ GeV/c^2 to $[3.30, 3.65]$ GeV/c^2 and $[3.25, 3.60]$ GeV/c^2 and the maximum differences in the fitted yields are considered as the associated systematic uncertainties. Regarding the peaking background contributions, the Σ^0 sideband ranges were changed from $[1.151, 1.172]$, $[1.213, 1.234]$ GeV/c^2 to $[1.153, 1.174]$, $[1.211, 1.232]$ GeV/c^2 and the difference in signal yields is taken as the systematic uncertainty. With regard to non-χ_{cJ} backgrounds, the fit function is changed from a second to a third order polynomial in the fit to the $\Sigma^0 \bar{p} K^+$ invariant mass distribution and the difference between the two fits is taken as the systematic uncertainty.

The systematic uncertainties due to the branching fractions of $\psi(3686) \to \gamma\chi_{c0}(\chi_{c1}, \chi_{c2})$, and $\Lambda \to p\pi^-$, are 2.0% (2.5%, 2.1%), and 0.8% according to the PDG [1]. For the $\Sigma^0 \to \gamma\Lambda$ decay, no uncertainty is given in the PDG.

The number of $\psi(3686)$ events is determined to be $(448.1 \pm 2.9) \times 10^6$ from inclusive hadronic events [11], thus the uncertainty is 0.6%.

All systematic uncertainty contributions discussed above are summarized in Table II. The total systematic uncertainty for each χ_{cJ} decay is obtained by adding all contributions in quadrature.

VII. SUMMARY

Using the $(448.1 \pm 2.9) \times 10^6$ $\psi(3686)$ events accumulated with the BESIII detector, the three-body decays of $\chi_{cJ} \to \Sigma^0 \bar{p} K^+$ $(J = 0, 1, 2)$ are studied for the first time,

and clear χ_{cJ} signals are observed. The branching fractions of $\chi_{cJ} \to \Sigma^0 \bar{p} K^+$ are determined to be $(3.03 \pm 0.12(\text{stat}) \pm 0.15(\text{syst})) \times 10^{-4}$, $(1.46 \pm 0.07(\text{stat}) \pm 0.07 \times (\text{syst})) \times 10^{-4}$, and $(0.91 \pm 0.06(\text{stat}) \pm 0.05(\text{syst})) \times 10^{-4}$ for $J = 0$, 1, and 2, respectively.

Comparing with the isospin conjugate decays of $\chi_{cJ} \to \Sigma^+ \bar{p} K_S^0$ ($J = 0, 1, 2$) [8], we obtain the ratios of the branching fractions $\frac{\mathcal{B}(\chi_{c0} \to \Sigma^0 \bar{p} K^+)}{\mathcal{B}(\chi_{c0} \to \Sigma^+ \bar{p} K_S^0)} = 0.86 \pm 0.06 \pm 0.06$, $\frac{\mathcal{B}(\chi_{c1} \to \Sigma^0 \bar{p} K^+)}{\mathcal{B}(\chi_{c1} \to \Sigma^+ \bar{p} K_S^0)} = 0.95 \pm 0.08 \pm 0.06$, and $\frac{\mathcal{B}(\chi_{c2} \to \Sigma^0 \bar{p} K^+)}{\mathcal{B}(\chi_{c2} \to \Sigma^+ \bar{p} K_S^0)} = 1.10 \pm 0.13 \pm 0.07$, respectively, where common sources of systematic uncertainties are canceled. These results are consistent with isospin symmetry within 1.6σ.

Although there is no evident intermediate resonances on two-body subsystems of χ_{cJ} decays, the mass distributions of two-body subsystems are not completely consistent with the phase-space MC simulations. This implies the existence of intermediate baryon resonances. With the present statistics, it is difficult to study them in detail and draw any conclusions to them. More $\psi(3686)$ events in the future in combination with advanced analysis technique, such as partial wave analysis, may shed light on the intermediate structures.

ACKNOWLEDGMENTS

[1] P. A. Zyla *et al.* (Particle Data Group), Prog. Theor. Exp. Phys. **2020**, 083C01 (2020).

[2] D. M. Asner *et al.*, Int. J. Mod. Phys. A **24**, 499 (2009).

[3] M. Ablikim *et al.* (BESIII Collaboration), Chin. Phys. C **44**, 040001 (2020).

[4] P. H. Eberhard, J. H. Friedman, M. Pripstein, and R. R. Ross, Phys. Rev. Lett. **22**, 200 (1969).

[5] M. Aguilar-Benitez, V. E. Barnes, D. Bassano, S. U. Chung, R. L. Eisner, E. Flaminio, J. B. Kinson, N. P. Samios, and K. Jaeger, Phys. Rev. Lett. **25**, 58 (1970).

[6] S. P. Apsell *et al.*, Phys. Rev. D **10**, 1419 (1974).

[7] J. J. M. Timmermans *et al.*, Nucl. Phys. **B112**, 77 (1976).

[8] M. Ablikim *et al.* (BESIII Collaboration), Phys. Rev. D **100**, 092006 (2019).

[9] M. Ablikim *et al.* (BESIII Collaboration), Nucl. Instrum. Methods Phys. Res., Sect. A **614**, 345 (2010).

[10] C. H. Yu *et al.*, in *Proceedings of IPAC2016, Busan, Korea, 2016*, https://doi.org/10.18429/JACoW-IPAC2016-TUYA01.

[11] M. Ablikim *et al.* (BESIII Collaboration), Chin. Phys. C **42**, 023001 (2018).

[12] S. Agostinelli *et al.* (GEANT4 Collaboration), Nucl. Instrum. Methods Phys. Res., Sect. A **506**, 250 (2003).

[13] S. Jadach, B. F. L. Ward, and Z. Wás, Comput. Phys. Commun. **130**, 260 (2000).

[14] S. Jadach, B. F. L. Ward, and Z. Wás, Phys. Rev. D **63**, 113009 (2001).

[15] R. G. Ping, Chin. Phys. C **32**, 599 (2008).

[16] D. J. Lange, Nucl. Instrum. Methods Phys. Res., Sect. A **462**, 152 (2001).

[17] J. C. Chen, G. S. Huang, X. R. Qi, D. H. Zhang, and Y. S. Zhu, Phys. Rev. D **62**, 034003 (2000).

[18] E. Richter-Was, Phys. Lett. B **303**, 163 (1993).

[19] M. Ablikim *et al.* (BESIII Collaboration), Phys. Rev. D **95**, 072004 (2017).

[20] M. Xu *et al.*, Chin. Phys. C **33**, 428 (2009).

[21] R. E. Mitchell *et al.* (CLEO Collaboration), Phys. Rev. Lett. **102**, 011801 (2009).

[22] M. Ablikim *et al.* (BESIII Collaboration), Phys. Rev. D **85**, 092012 (2012).

[23] M. Ablikim *et al.* (BESIII Collaboration), Phys. Rev. D **83**, 112005 (2011).

[24] M. Ablikim *et al.* (BESIII Collaboration), Phys. Rev. D **92,** 052003 (2015).

[25] M. Ablikim *et al.* (BESIII Collaboration), Phys. Rev. D **87,** 012007 (2013).

[26] M. Ablikim *et al.* (BESIII Collaboration), Phys. Rev. D **87,** 012002 (2013).

[27] V. V. Anashin *et al.* (KEDR Collaboration), Int. J. Mod. Phys. Conf. Ser. **02,** 188 (2011).